

Supporting Information

Lubricant-mediated strong droplet adhesion on lubricant-impregnated surfaces

Jiaqian Li¹, Wei Li¹, Xin Tang¹, Xing Han¹ and Liqiu Wang^{1*}

¹*Department of Mechanical Engineering, The University of Hong Kong, Hong Kong, 999077, China*

*Correspondence and requests for materials should be addressed to L.W. (lqwang@hku.hk)

This supporting information includes:

Table S1. Properties of the different lubricants used in our experiments.

Figure S1. Fluorescence detection of the liquid residue.

Figure S2. Characterization of nanostructures on the micropost surface.

Figure S3. Contact angle characterization of superhydrophobic surfaces.

Figure S4. Wettability characterization of lubricant-infused surfaces.

Figure S5. Contact angle measurement of the LISs infused by different GPL oils with varying viscosity.

Figure S6. Contact angle measurement of the LISs with different wettability for water droplet.

Figure S7. Droplet adhesion test on a lubricant bath.

Figure S8. The effect of the droplet detachment speed on the droplet adhesion.

Figure S9. Successive snapshots of the droplet shedding from the hydrophilic lubricant-infused mesh.

Figure S10. Successive images showing the roll-off droplet shedding from the superhydrophobic mesh.

Figure S11. Successive images showing the jump-off droplet shedding from the superhydrophobic mesh.

Figure S12. Representative image demonstrating the shedding of small droplets from the superhydrophobic mesh.

Figure S13. Time-dependent curves of fog collection weights.

Captions of Supplementary Movies from S1 to S8

Table S1. Properties of the different lubricants used in our experiments. Properties are taken from manufacturer data sheets, MSDS or reporting reference.

Lubricant	Density (g/cm ³)	Lubricant/air surface tension (mN/m)	Viscosity (cSt)
Krytox GPL 100	1.87 ^a	16-20 ^a	12.4 ^a
Krytox GPL 102	1.91 ^a	16-20 ^a	38 ^a
Krytox GPL 103	1.92 ^a	16-20 ^a	82 ^a
Krytox GPL 105	1.94 ^a	16-20 ^a	522 ^a
Silicone oil	0.95 ^b	21 ^a	20 ^a
Mineral oil	0.84 ^b	30 ^a	15.3 ^b
Hydroxy-terminated polydimethylsiloxane (PDMS65)	0.97 ^b	21.67 ^b	65 ^a
Hydroxy-terminated polydimethylsiloxane (PDMS25)	0.95 ^b	21.28 ^b	25 ^a

^a At 20 °C, unless specified otherwise. ^b At 25 °C.

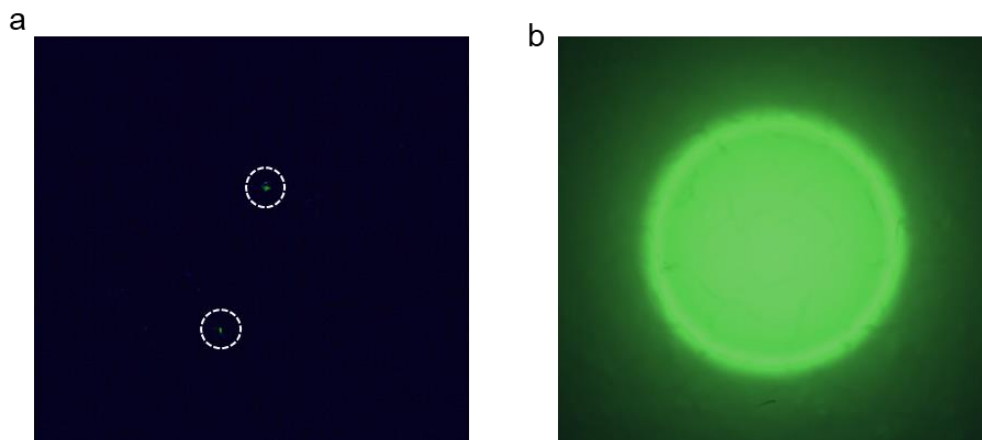


Figure S1. Fluorescence detection of the liquid residue. (a) Fluorescence image showing the liquid residue after adhesion test on the superhydrophobic TiO_2 surface. Dash circles indicate the liquid residues detected on the superhydrophobic surface. (b) Fluorescence image of the residual droplet after adhesion on the lubricant-infused surface. A small droplet adheres to the lubricant-infused surface.

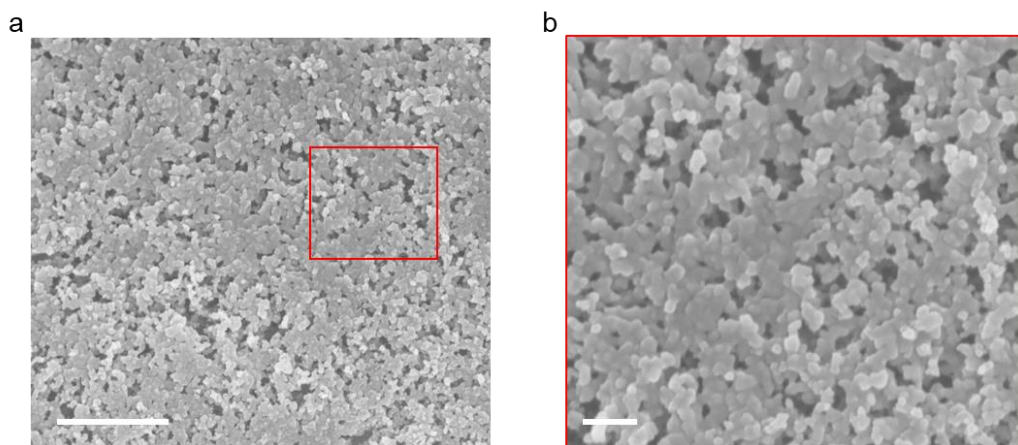


Figure S2. Characterization of nanostructures on the micropost surface. (a) Representative SEM image of the nanoparticles for the immobilization of the lubricant on the micropost surface. (b) Magnified SEM image of the nanoparticles corresponding to the red rectangle in (a). Scale bars: (a) 1 μm and (b) 200 nm.

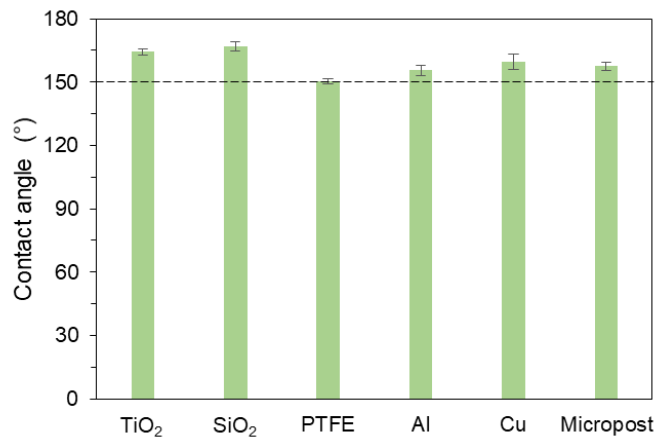


Figure S3. Contact angle characterization of superhydrophobic surfaces. The apparent contact angles of these surfaces are equal to or greater than 150°, which is suitable to prepare the lubricant-infused surfaces.

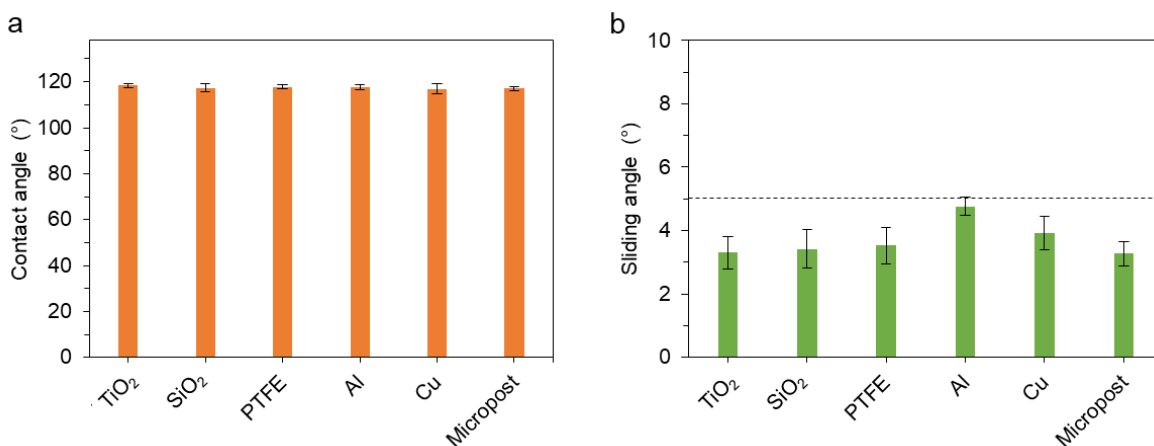


Figure S4. Wettability characterization of lubricant-infused surfaces. (a) The apparent contact angles on different LISs. These LISs have similar apparent contact angles regardless of the underlying superhydrophobic surfaces. (b) The sliding angles on different LISs. The sliding angles on these LISs are smaller than 5°.

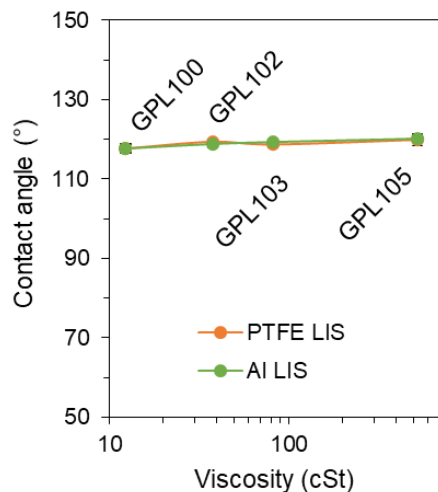


Figure S5. Contact angle measurement of the LISs infused by different GPL oils with varying viscosity. Since GPL oils have similar surface tension, the contact angles on these LISs infused by different GPL oils are approximately equal to 118°.

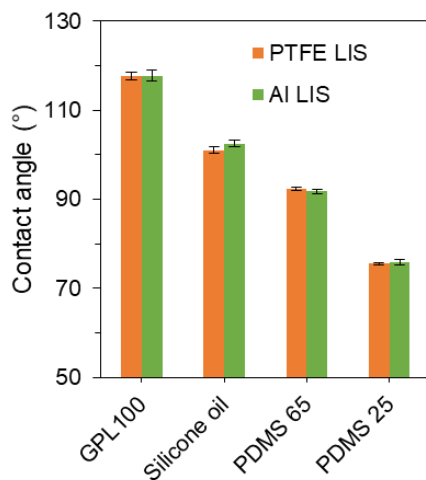


Figure S6. Contact angle measurement of the LISs with different wettability for water droplet. The LISs with different contact angles ranging from ~ 118° to ~ 76° are prepared to investigate the effect of wettability on the droplet adhesion.

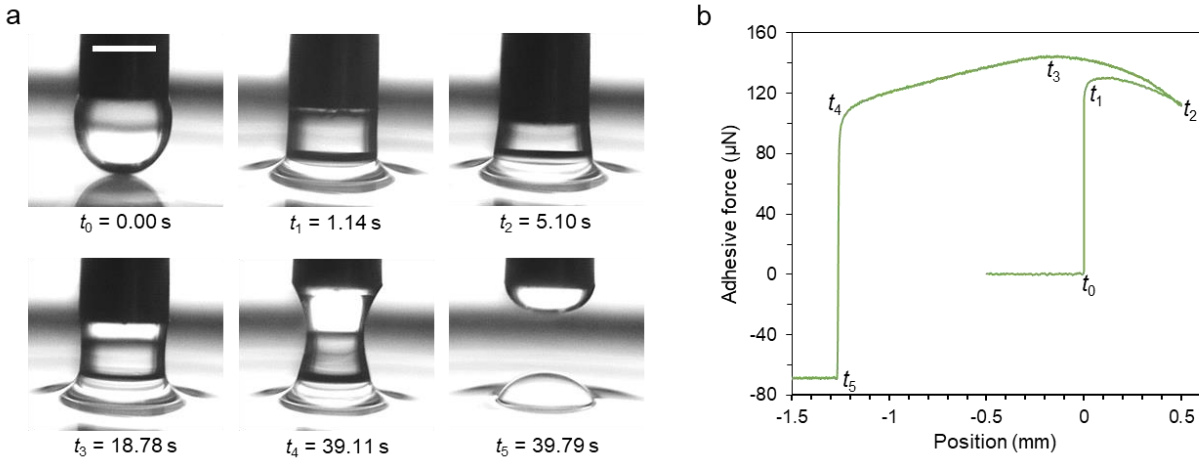


Figure S7. Droplet adhesion test on a lubricant bath. (a) Successive snapshots of the adhesion test of a droplet ($\sim 10 \mu\text{l}$) on a deep GPL 100 oil bath. The depth of the oil is greatly larger than the diameter of the tested droplet. Jump-in and Jump-off instabilities are also detected during droplet adhesion on such oil bath, analogous to those in the droplet adhesion on the lubricant-infused surface. After lifting the droplet up from the bath, an offspring droplet is also floating on the bath surface. (b) Force-displacement curve of the droplet adhesion on the oil bath corresponding to (a). Here t_0 , t_1 , t_2 , t_3 , t_4 and t_5 indicate the places of corresponding snapshots in (a). Scale bar: (a) 2 mm.

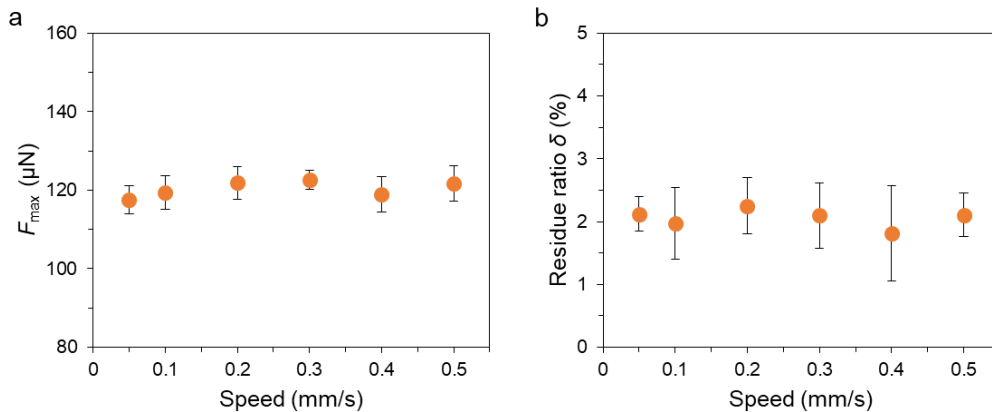


Figure S8. The effect of the droplet detachment speed on the droplet adhesion. (a) The variation of F_{max} under a function of the detachment speed of the droplet from the PTFE LIS. (b) The variation of δ under a function of the detachment speed of the droplet from the PTFE LIS.

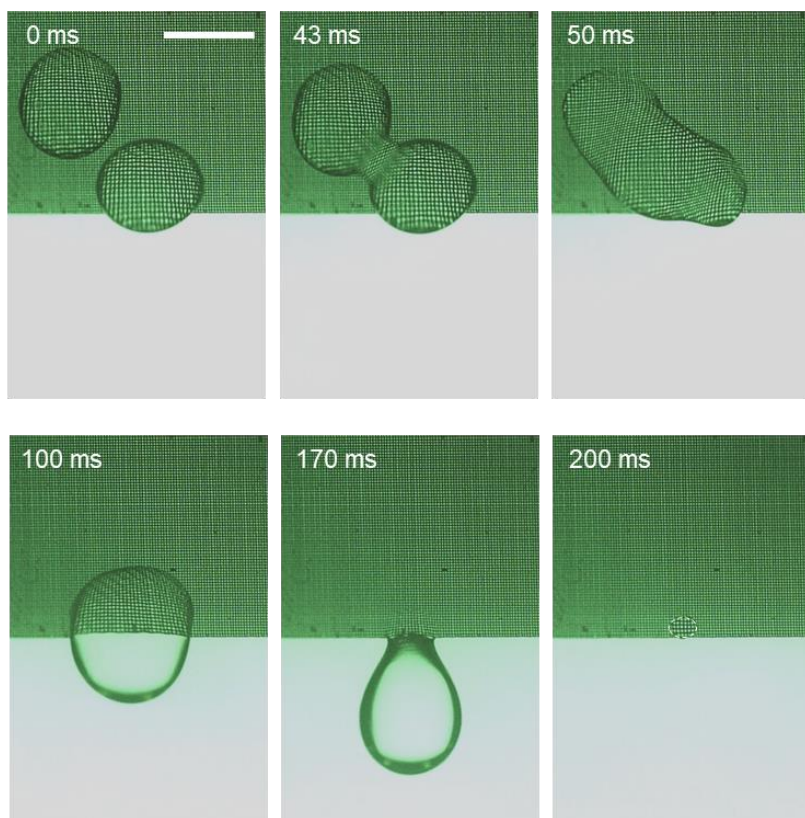


Figure S9. Successive snapshots of the droplet shedding from the hydrophilic lubricant-infused mesh. Analogous to the hydrophobic lubricant-infused mesh, the intercepted droplet detaches from the mesh by droplet coalescence, after which a residual droplet is generated as marked by the white dashed circle. Scale bar is 2 mm.

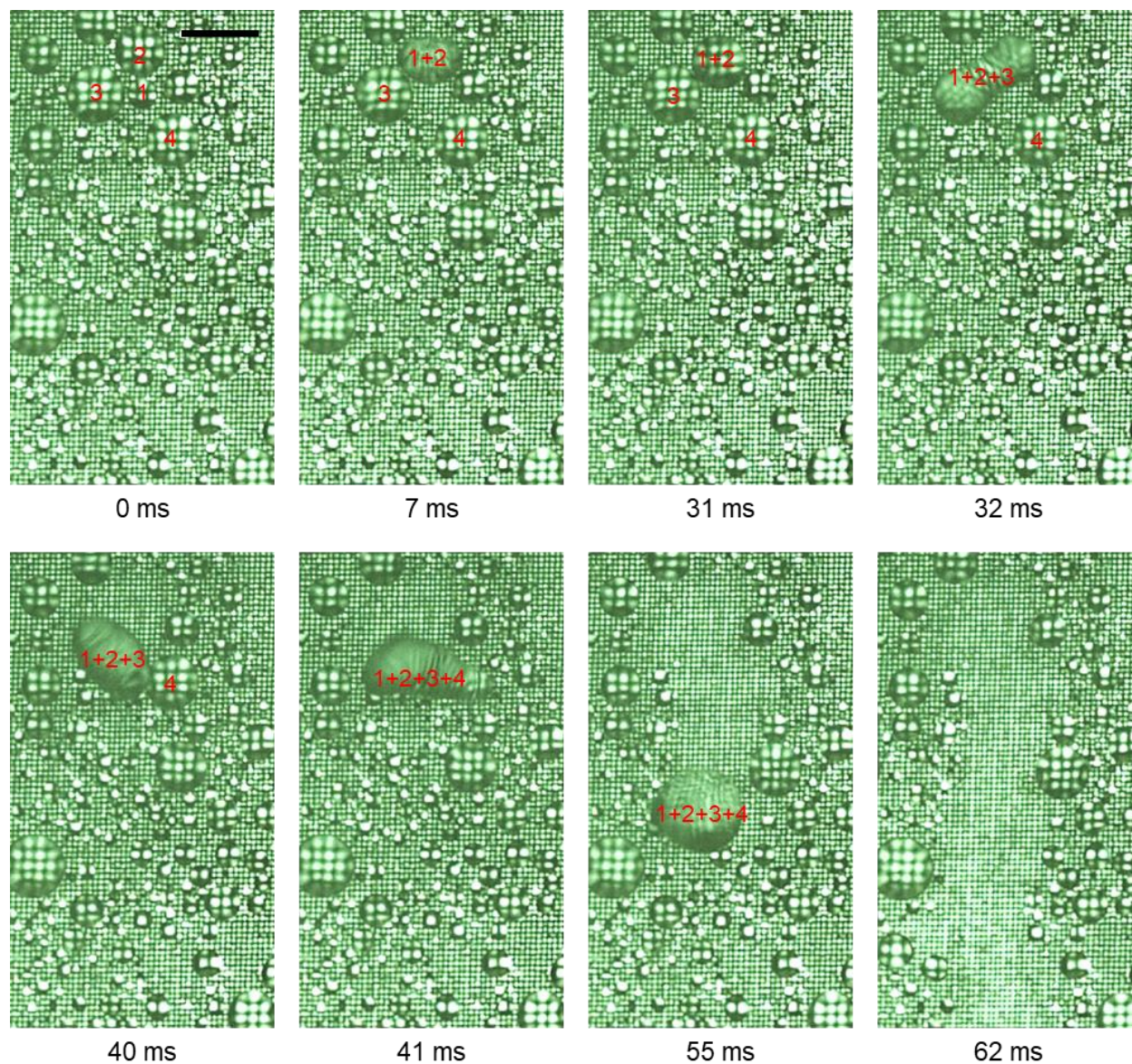


Figure S10. Successive images showing the roll-off droplet shedding from the superhydrophobic mesh. The droplet 1 first coalesces with the droplet 2 (7 ms), and then with the droplet 3 (32 ms), and finally with the droplet 4 (41 ms). Such successive droplet coalescences make the droplet 1+2+3+4 rolling down along the mesh, during which the big droplet merges with many smaller droplets (41 to 62 ms). As a result, there are no droplets remaining in the route where the detached droplet rolls, which effectively dries the mesh beneficial for the continuous interception of the mist droplets. Scale bar is 1 mm.

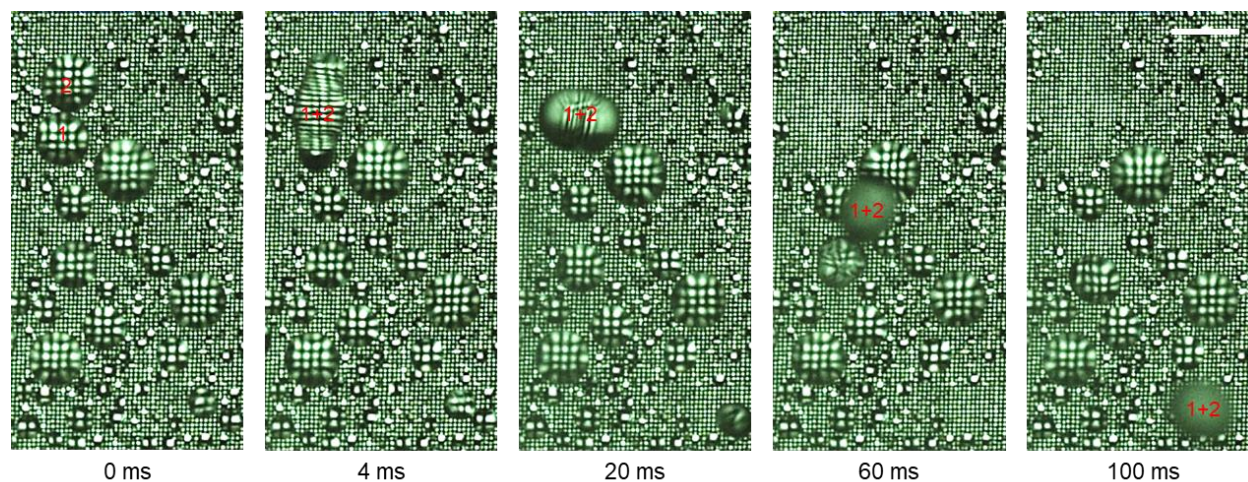


Figure S11. Successive images showing the jump-off droplet shedding from the superhydrophobic mesh. The droplet 1 coalesces with the droplet 2, which converts the excessive surface energy to the kinetic energy to enable the merged droplet 1+2 jumping off from the mesh. As such, small droplets, even microscale droplets, can be collected by the superhydrophobic mesh through the jump-off shedding mechanism. Scale bar is 1 mm.

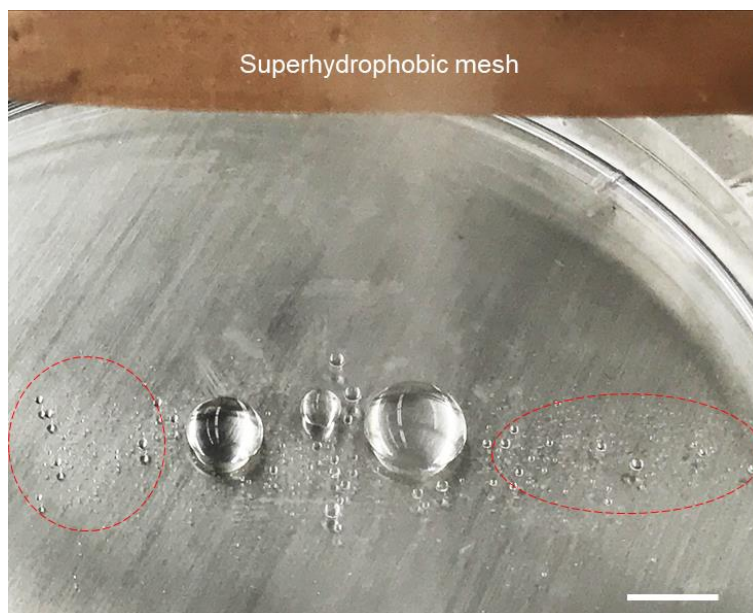


Figure S12. Representative image demonstrating the shedding of small droplets from the superhydrophobic mesh. The droplet coalescence can cause many microscale droplets to detach from the superhydrophobic mesh. Note that these microscale droplets cannot be detected owing to the limitation of the balance precision. Scale bar is 5 mm.

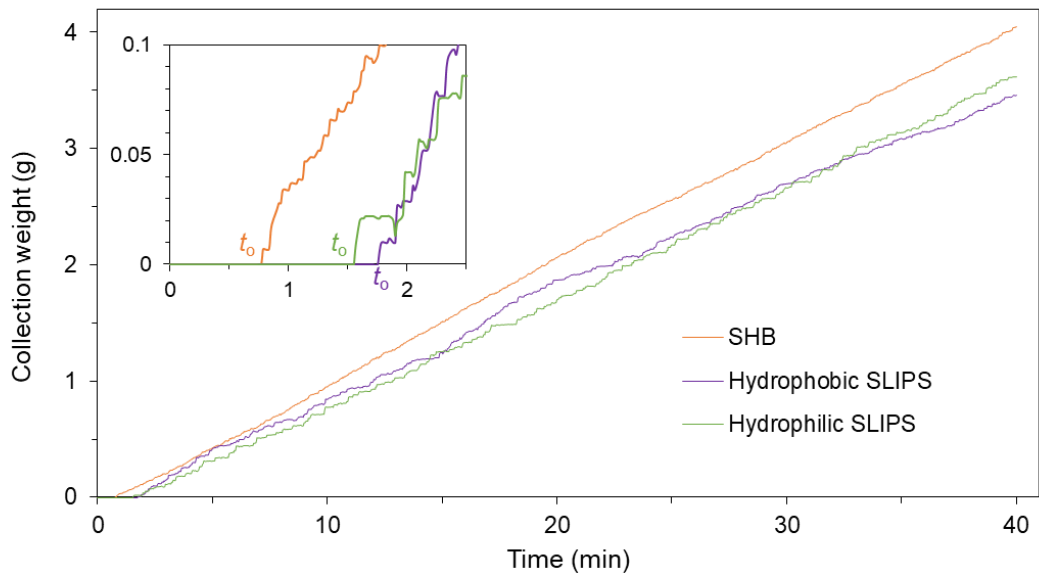


Figure S13. Time-dependent curves of fog collection weights. The orange, purple and green curves denote the SHB, hydrophobic SLIPS, and hydrophilic SLIPS meshes, respectively. The inset plot shows the onset times t_0 on these three meshes. Here the onset time is defined as the time for the first droplet to detach from the mesh.

Captions of Supplementary Movies

Movie S1. Droplet adhesion test on the superhydrophobic surface. The superhydrophobic TiO₂ surface shows a small droplet adhesion, with almost no residue when a water droplet detaches from it.

Movie S2. Droplet adhesion test on the lubricant-infused surface. The lubricant-infused surface shows a relatively strong adhesion when a water droplet detaches from it. A small residual droplet is generated owing to the adhesion between the droplet and the lubricant, when the tested droplet detaches from the lubricant-infused surface.

Movie S3. Droplet contact dynamics on the lubricant-infused surface. When a droplet (~ 10 μl) with FITC-BSA contacts the lubricant-infused surface, the lubricant rises around the droplet base owing to the capillary action, resulting in the formation of lubricant ridge.

Movie S4. Droplet detachment dynamics from the lubricant-infused surface. With the retraction of the droplet with FITC-BSA, the lubricant ridge around the droplet base is gradually stretched, followed by the rupture of the droplet. Finally, a small descendent droplet resides on the lubricant-infused surface.

Movie S5. Photoelectrically triggered droplet manipulation on the lubricant-infused surface. Under the irradiation of a 785-nm laser, a water droplet (~ 10 μl) moves on the lubricant-infused surface toward the region where the laser irradiates owing to the photo-induced electric field.

Movie S6. Magnetically triggered droplet manipulation on the lubricant-infused surface. When a small magnet with 80 mT is applied, a ferrofluid droplet (~ 10 μl) moves directionally without any residue on the lubricant-infused surface toward the magnet.

Movie S7. Magnetically triggered droplet transfer from the lubricant-infused surface. When the ferrofluid droplet is transferred away from the lubricant-infused surface, a small ferrofluid droplet would stick stably to the surface.

Movie S8. Droplet shedding from the hydrophobic lubricant-infused mesh. Small droplet first stays at the mesh edge due to the lubricant-induced adhesion, and then detaches from the mesh by virtue of droplet coalescence. But a residual droplet is produced with the shedding of the droplet from the mesh.